

Large variation in the boundary-condition slippage for a rarefied gas flowing between two surfaces

J. Laurent, A. Drezet, H. Sellier, J. Chevrier and S. Huant

Institut Néel, CNRS and Université Joseph Fourier, BP 166, F-38042 Grenoble Cedex 9, France

(Dated: January 22, 2022)

We study the slippage of a gas along mobile rigid walls in the sphere-plane confined geometry and find that it varies considerably with pressure. The classical no-slip boundary condition valid at ambient pressure changes continuously to an almost perfect slip condition in a primary vacuum. Our study emphasizes the key role played by the mean free-path of the gas molecules on the interaction between a confined fluid and solid surfaces and further demonstrates that the macroscopic hydrodynamics approach can be used with confidence even in a primary vacuum environment where it is intuitively expected to fail.

PACS numbers: 47.15.Rq, 47.10.ad, 47.61.Fg, 07.79.Lh

It is traditionally assumed [1] that in a fluid flowing along a solid surface, molecules nearest to the surface are globally stopped due to friction and collisions. This so called no-slip boundary condition has been very successful in modeling macroscopic experiments and it indeed forms one of the fundamental axiom of classical hydrodynamics. However, it has recently been recognized that this standard condition is often not valid at submicro- and nanoscales [2, 3]. Furthermore, the hydrodynamic behavior close to a solid surface changes drastically with interfacial phenomena like roughness or surface chemistry and the exact physics underlying these variations is not well understood [2–5]. Beyond its fundamental interest, elucidating these boundary conditions becomes a key issue for micro- and nano-electromechanical systems (MEMS-NEMS) such as sensors and actuators working in fluidic environments (liquid or gas). Although important results have been reported in a liquid environment (e.g. flow through nano- and microchannels or nano-tribology [2, 3, 6, 7]) there are only a few indications to the significance of these phenomena in gases [8, 9, 12–14].

In this letter, we analyze a simple model apparatus able to continuously tune in the sphere-plane confined geometry the slippage boundary conditions at the solid-gas interface. By decreasing the surrounding pressure of a sphere facing a rigid wall in a gas (air or Helium), we find that these boundary conditions continuously evolve from a viscous regime supporting no slip to a ballistic regime with perfect slip. We interpret our results in terms of a giant modification of the gas slippage at the interfaces. Therefore, our experiments appear to reconcile in a single setup boundary conditions that look conflicting at first sight.

The experimental setup (Fig. 1) is a homemade atomic force microscope (AFM) working at 300 K under controlled atmosphere. An optical-fiber based interferometric detection of the cantilever [12, 15] provides the required sensitivity to measure the impact of gas confinement on the viscous damping of the probe. The latter is a 460 μm long, 50 μm wide, and 2 μm thick, silicon AFM microlever with a $R = 20 \mu\text{m}$ radius polystyrene sphere glued at its extremity. In order to control the electrostatic interaction (see below), the whole probe

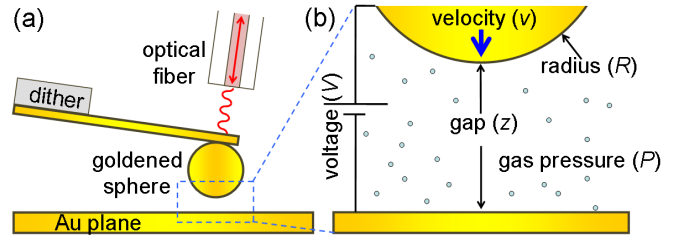


FIG. 1: (a) Scheme of the experimental setup. (b) Zoom on the interaction zone between the facing surfaces defining the relevant physical parameters.

(i.e. cantilever and sphere) is coated with a 200 nm thick gold layer, and the AFM chip is glued with silver paint on a holder attached to the microscope frame. The probe spring constant $k = 0.45 \text{ N/m}$ and the resonance frequency $f_0 = 9420 \text{ Hz}$ have been measured using the Brownian motion of the thermally actuated lever at 300 K [12, 14]. The planar surface facing the sphere is a silicon substrate coated with a 200 nm thick gold layer and mounted on a high-precision positioning system to adjust the cavity gap z between the sphere and the sample. An inertial motor makes sub-micron steps over a large 7 mm displacement range, whereas a piezo-scanner corrected for hysteresis distortions ensures a fine vertical positioning over a 1.5 μm range.

For our measurements, it is important to conceive a method for measuring the absolute gap z . This is achieved by applying a voltage bias V to the probe with respect to the facing flat surface as commonly done in Casimir force measurements where contact between facing surfaces must be avoided [15, 16]. The cantilever is mechanically actuated with a dither at its resonant frequency using a phase-locked loop device and the resonant frequency shift $\Delta f = \alpha (V - V_c)^2$ is recorded as a function of V to extract the coefficient α that bears the desired distance information (V_c is the difference in materials work functions). For $z \ll R$ in the sphere-plane geometry, we use the relation $\alpha \approx f_0 \pi \epsilon_0 R / (2kz^2)$ to find the absolute distance z . In fact, to reach a better precision of 2% on z , we record α during a precise 1.5 μm scan around the mean position and fit the results against the

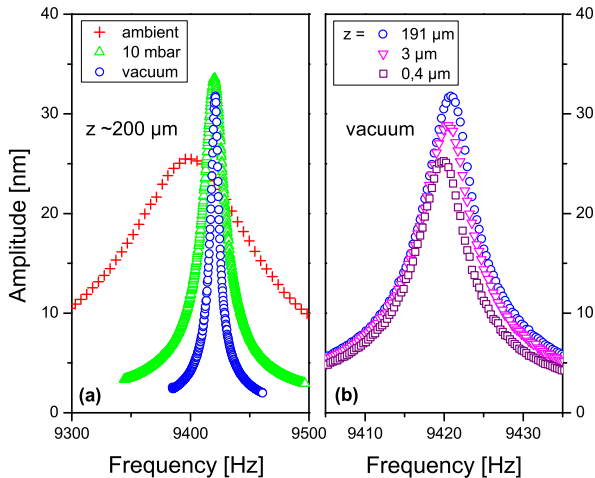


FIG. 2: (a) Resonance spectra of the cantilever-sphere probe at three different pressures: ambient (1 bar), helium gas (10 mbar), and vacuum (4×10^{-2} mbar), when the fluid is not confined (the sphere to surface distance is $z \approx 200 \mu\text{m}$). Note that the mechanical excitation has been reduced at low pressure to keep a similar amplitude at resonance. (b) Resonance spectra of the probe in vacuum for three different gaps z . The resonance width, i.e. damping factor, increases with decreasing separation.

above formula.

We have measured the vibration amplitude A as function of the excitation frequency f for three gas pressures P and several distances z . Examples of resonance curves are shown in Fig. 2(a) at large distance and for different pressures and in Fig. 2(b) for different distances in a primary vacuum. By fitting each curve with the Lorentzian response of an harmonic oscillator:

$$A[f] = A_0 \frac{\gamma f_0}{\sqrt{(f_0^2 - f^2)^2 + \gamma^2 f^2}} \quad (1)$$

we obtain the dissipation constant $\Gamma = k\gamma/(2\pi f_0^2)$ of the probe, with a fitting error smaller than 1%. The results are shown on the left graphs of Fig. 3 for three pressure conditions: (a) air at atmospheric pressure (1000 mbar), (b) helium at low pressure (10 mbar), and (c) air vacuum (4×10^{-2} mbar).

When the sphere is far from the sample, the damping factor reaches a constant value Γ_0 , characterizing the dissipation of the {cantilever + sphere} oscillating system in the fluid. This value is directly extracted from the data and reported in Table I (except in vacuum where the damping factor is not saturated at the largest distance and Γ_0 was obtained by fitting with Eq. 3 as described below). As is also visible in Fig. 2(a), Γ_0 decreases with decreasing pressure P in agreement with previous works [9–11]. In the viscous regime this is mainly due to the existence of a boundary layer of thickness $\delta_B \propto 1/\sqrt{P}$ [1, 17] representing a dissipation channel at finite frequency that adds to the intrinsic losses Γ_{int} of the lever (i.e. losses in the limit $f_0 \rightarrow 0$): $\Gamma_0 = \Gamma_{\text{int}} + O(\sqrt{P})$ [9–11].

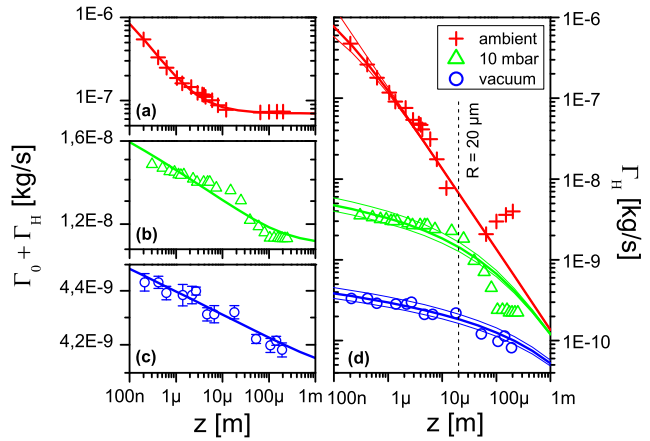


FIG. 3: (a-c) Evolution of the damping factor $\Gamma(z) = \Gamma_0 + \Gamma_H(z)$ as a function of the gap z between the sphere and the plane at three pressures: (a) ambient air at 1 bar, (b) helium gas at 10 mbar, and (c) air vacuum at 4.10^{-2} mbar. The symbols represent the data (at 1 bar and 10 mbar, the experimental error bars are within the symbol size) and the continuous lines are the fitting curves according to the theoretical model. (d) Evolution of $\Gamma_H(z)$ with the gap z using the same color code as (a-c). The two curves (thin lines) surrounding each fitting curve (thick lines) provide an error estimate on the slip length b (from top to bottom: $b = 0, 0.05, 0.1, 55, 70, 85, 1000, 1200, 1400 \mu\text{m}$).

Gas	P [mbar]	Γ_0 [kg/s]	b [μm]	λ_m [μm]	p_d
Air	1000	7.0×10^{-8}	0.05	0.06	0.9
He	10	1.12×10^{-8}	70	10	0.17
Air	0.04	4.1×10^{-9}	1200	2500	1.2

TABLE I: Measured slip length b and asymptotic damping rate Γ_0 together with the calculated mean free-path λ_m and accommodation coefficient p_d (see Eq. 4) at each pressure P .

When the gap decreases, the hydrodynamic force due to the gas confinement contributes a z -dependent additional dissipation channel $\Gamma_H(z)$ such that $\Gamma(z) = \Gamma_0 + \Gamma_H(z)$. The central result of our work is shown in Fig. 3(d) where $\Gamma_H(z)$ is plotted for different pressures. It is clearly seen that the dissipation observed at small distance is strongly reduced at low pressure. If in agreement with usual statistical mechanics [1] we accept that the fluid viscosity η does not depend on pressure (a reasonable assumption in the viscous regime) we can conclude that the boundary conditions at the solid-fluid interface should strongly change with pressure. In other words, the so-called slip-length b , usually used to characterize the fluid flow at the interface [3, 4, 6], varies by a large amount. b is related to the fluid velocity gradient at the solid surface by $v|_{\text{surface}} = b \partial v / \partial z|_{\text{surface}}$ (where v is the tangential fluid velocity) and can equivalently be interpreted as the fictitious depth below the surface where the no-slip boundary conditions would be satisfied.

In the sphere-plane geometry with no-slip boundary conditions (i.e. $b \sim 0$), the dissipation constant $\Gamma_H(z)$ is

given in the limit $z \ll R$ by the Taylor formula [1, 6]:

$$\Gamma_H(z) = \frac{6\pi\eta R^2}{z} \quad (2)$$

where η is the dynamic viscosity which does not change with pressure ($1.8 \times 10^{-5} \text{ kg}\cdot\text{m}^{-1}\cdot\text{s}^{-1}$ for air and $1.9 \times 10^{-5} \text{ kg}\cdot\text{m}^{-1}\cdot\text{s}^{-1}$ for Helium). To take into account the gas slippage at the boundaries, we follow the reasoning of Hocking [18] and Vinogradova [19] and introduce a correction function f^* such that

$$\Gamma_H(z) = \frac{6\pi\eta R^2}{z} f^*\left(\frac{z}{6b}\right) \quad (3)$$

with $f^*(x) = 2x \left[(1+x) \ln\left(1 + \frac{1}{x}\right) - 1 \right]$. In this formula (obtained for an incompressible fluid in the laminar regime [20]) we assume the same values for b on both surfaces since the two walls are coated with the same material. By fitting the three sets of data in Fig. 3(d) with Eq. 3 in the range $z < 20 \mu\text{m}$, we determine a slip length b for each pressure. Note that b is the only free parameter in the fit, except for the data in vacuum where both Γ_0 and b are simultaneous adjustable parameters. b is however not sensitive to the choice of Γ_0 since b is determined essentially by the absolute changes of $\Gamma(z)$. The results are presented in Table I with an estimation of the error shown in Fig. 3(d). The strong increase of b at lower pressure clearly shows that the friction of the confined fluid along the solid boundaries considerably changes with pressure going from the usual no-slip condition in ambient air (i.e. Γ_H follows a $1/z$ law) to a quasi-perfect slip regime at low gas pressure (i.e. $\Gamma_H \propto -\ln(z/b)/b$).

In order to visualize the impact of a finite b on the fluid dynamics close to the surface, we compute the (radial) fluid velocity profile $v(Z)$ in the gap z between the two surfaces using the analytical theory of [18, 19]. Due to the fluid incompressibility and the limit $z \ll R$, the fluid is essentially ejected from the gap in the radial direction in response to the vertical displacement of the sphere [21]. The comparison between the three different values of b obtained in the experiment (see Table I) is shown in Fig. 4. We clearly switch from the usual Poiseuille parabolic velocity profile (i.e. $v \sim 0$ on the solid boundary) for $b \rightarrow 0$, to a quasi-constant velocity profile in the gap for $b \rightarrow +\infty$. Therefore our experiment reveals a continuous transition between these extreme regimes.

Now, from a microscopic point of view, the slippage coefficient is linked to the very nature of the interaction between moving surfaces and air molecules. Following the historical approach of Maxwell's kinetic theory of gases [22], two interaction channels can be distinguished: a specular one where molecules collide elastically with the surface and a diffusive one where molecules are reflected diffusively by the wall. The slip length b in this statistical model is given by the Maxwell formula [14, 22–24]:

$$b \simeq \frac{2}{3} \lambda_m \frac{2 - p_d}{p_d} \quad (4)$$

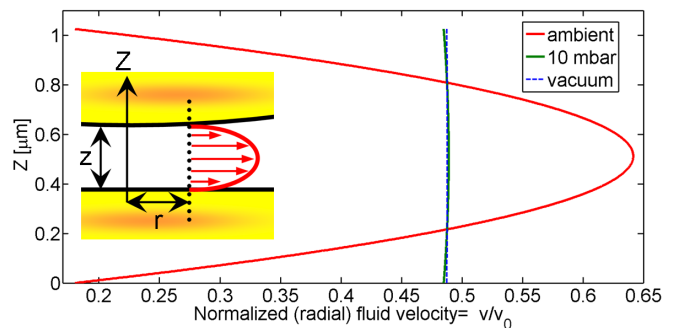


FIG. 4: The normalized radial fluid velocity profile $v(Z, r)/v_0$ (v_0 is the sphere velocity) as function of the coordinate Z in a $z = 1 \mu\text{m}$ gap and for a radial coordinate $r = 1 \mu\text{m}$. The profiles are calculated for the three b values of Table I.

where λ_m is the typical mean free-path of gas molecules and p_d the tangential momentum accommodation coefficient, i.e. the fraction of those particles hitting the surface with a diffusive reflection.

The main dependence of b with pressure comes from the molecular mean free-path (see Table I): $\lambda_m = \frac{k_B T}{\sqrt{2} \sigma P}$ where T is the temperature, k_B the Boltzmann's constant, and σ the molecular cross-section. Two important asymptotic regimes are clearly found in the experiment (see Fig. 4). On the one hand, when the mean free-path is extremely small compared to other macroscopic dimensions (i.e. at ambient air pressure), the fluid particles interact strongly with themselves, and even more strongly with surfaces located within a characteristic distance given by λ_m . This is a consequence of multiple collisions, reflections, and adsorption processes [2–4, 22]. In this diffusive regime, the tangential velocity of the molecules decreases at short distance from the surface, such that the slip-length b tends to zero and the no-slip condition applies. On the other hand, when the mean free-path is considerably larger than the gap, the molecules interact mainly with surfaces and there is no momentum transfer among the molecules themselves. In this ballistic or molecular flow regime, the velocity gradient vanishes at the surface. This results in a giant slip length b .

In Eq. 4, the accommodation coefficient p_d (see Table I) depends on the surface properties and gas density (i.e. on the probability of multiple collisions). Recent analysis based on the fluctuation-dissipation theorem and the Green-Kubo relation emphasize the importance of several microscopic parameters such as surface roughness and surface defects on the molecular dynamics close to the surface [3–6]. In our experiment, the rms roughness of the gold surfaces was found by AFM to be $\delta_r \simeq 3 \text{ nm}$ for both the sphere and sample. This certainly contributes to increase p_d and reduce b as compared to a perfect surface.

Note that Eq. 3 is an analytical solution of the Navier-Stokes equations whose validity is well established when the fluid density is sufficiently large to provide a local equilibrium within the fluid. However, in the present

experiment in vacuum, the mean free-path λ_m is much larger than any other relevant length (e.g. the gap z) so that the system enters in a molecular flow regime which should be discussed within the more general frame of Boltzmann's kinetic equations [1, 2]. Therefore, the slip length b deduced from our data at low pressure should be considered as an extrapolation showing the limitation of the usual hydrodynamic approach. Because the low-pressure data of Fig. 3 are well reproduced in our analysis, our work stresses the remarkable robustness of the Navier-Stokes Eq. 3 even in this molecular regime.

Finally, it is worth commenting on the differences between the present sphere-plane experiment and recent results obtained in a plane-plane geometry [12]. At atmospheric pressure, we obtain here a small slip length in agreement with Refs. [8, 16] whereas Ref. [12] reports on a perfect slip in the same fluid (air). One of the difference is the geometry, which is indeed known to be a critical parameter at micro- and nanoscales [2, 3, 10, 14, 25]. Another difference in Ref. [12] is the probe velocity which resulted from the thermal motion of the cantilever with oscillation amplitude $A \approx 0.05$ nm, whereas the probe is here mechanically actuated i.e. $A \approx 30$ nm (in the same context compare Refs.[13] and [8]). In addition, the surface roughness was only a few Angstroms, resulting in a smaller accommodation coefficient p_d and a larger slip-length b .

In conclusion, we have discovered that the slippage of a gas along mobile rigid walls varies considerably with pressure in the sphere-plane confined geometry. The classical no-slip boundary condition valid at ambient pressure changes continuously to an almost perfect slip condition in vacuum. This study emphasizes the key role played by the mean free-path λ_m on the interaction between a fluid and solid surfaces and demonstrates that the macroscopic hydrodynamics approach can be used with confidence even in good vacuum conditions. We anticipate that our work will have an impact on the MEMS and NEMS engineering and will motivate further fundamental studies of the physics of gas slippage along solid and mobile surfaces.

We are grateful to K. Joulain and O. Arcizet for helpful discussions and to A. Mosset and J. -F. Motte for valuable assistance during the experiments. This research was supported by the PNANO 2006 program of the Agence Nationale de la Recherche under the project name "MONACO".

[1] G. K. Batchelor, *Fluid dynamics*, (Cambridge University Press, Cambridge (UK) 1974).

[2] P. Tabeling, *Introduction to microfluidics* (Oxford University Press, USA, 2006).

- [3] E. Lauga, in *Handbook of Experimental Fluid Dynamics* edited by J. Foss, C. Tropea, and A. Yarin (Springer, New York, 2007), Chap. 19, p. 1219-1240.
- [4] L. Bocquet and E. Charlaix, *Chem. Soc. Rev.* **39**, 1073 (2010).
- [5] S. Guriyanova, B. Semin, T.S Rodrigues, H.-J. Butt, and E. Bonaccorso, *Microfluid. Nanofluid.* **8**, 653 (2010).
- [6] C. Neto, D. R. Evans, E. Bonaccorso, H.-J. Butt, and V. S. J. Craig, *Rep. Prog. Phys.* **68**, 2859 (2005).
- [7] O. I. Vinogradova and G. E. Yakubov, *Phys. Rev. E* **73**, 045302 (2006).
- [8] A. Maali and B. Bhushan, *Phys. Rev. E* **78**, 027302 (2008).
- [9] S. S. Verbridge, R. Ilic, H. G. Craighead, and J. M. Parpia, *Appl. Phys. Lett.* **93**, 013101 (2008).
- [10] M. Li, H. X. Tang, and M. L. Roukes, *Nat. Nanotechnol* **2**, 114 (2007).
- [11] O. Svitelskiy, V. Sauer, N. Liu, K.-M. Cheng, E. Finley, M. R. Freeman, and W. K. Hiebert, *Phys. Rev. Lett* **103**, 244501 (2009).
- [12] A. Siria, A. Drezet, F. Marchi, F. Comin, S. Huant, and J. Chevrier, *Phys. Rev. Lett* **102**, 254503 (2009).
- [13] C.D.F. Honig and W. A. Ducker, *J. Phys. Chem. C*, **114** 20114 (2010)
- [14] A. Drezet, A. Siria, S. Huant, and J. Chevrier, *Phys. Rev. E* **81**, 046315 (2010).
- [15] G. Jourdan, A. Lambrecht, F. Comin, and J. Chevrier, *Europhys. Lett.* **85**, 31001 (2009).
- [16] S. de Man, K. Heeck, R. J. Wijngaarden, and D. Iannuzzi, *Phys. Rev. Lett.* **103**, 040402 (2009).
- [17] The boundary layer $\delta_B = \sqrt{\nu/f_0}$, where ν is kinematic viscosity [1], is typically 20 μm at ambient pressure and reaches a few mm in vacuum.
- [18] L. M. Hocking, *J. Eng. Math.* **7**, 207 (1973).
- [19] O. Vinogradova, *Langmuir* **11**, 2213 (1995).
- [20] A typical value for the Reynolds number in our experiments is $Re \sim f_0 A z / \nu \simeq 10^{-5} - 10^{-6}$ at ambient pressure. At lower pressure this number is even reduced proportionally to pressure. This justifies our assumption of a laminar regime. Similarly, the gas incompressibility hypothesis is fully justified since the Mach number $M \sim f_0 A / c \simeq 10^{-6} \ll 1$ (c is sound velocity) is very small.
- [21] Here we have applied the Taylor formula (Eq. 2 and its extension Eq. 3) to z values exceeding the sphere radius R although it is valid in the limit $z \ll R$ only, so that our approach reveals general trends at large distances, rather than offering an accurate quantitative analysis. Similarly, the small tilt angle ($\simeq 10^\circ$) of the vibrating cantilever with respect to the plane surface (Fig. 1) results in a small horizontal velocity (18% of the main vertical velocity) that we neglect, but this does not change the orders of magnitude discussed here.
- [22] J. C. Maxwell, *Philos. Trans. R. Soc. London, Ser. B* **170**, 231 (1879).
- [23] F. Sharipov and D. Kalempa, *Phys. Fluids* **15**, 1800 (2003).
- [24] M. Fichman and G. Hetsroni, *Phys. Fluids* **17**, 123102 (2005).
- [25] A. Siria, S. Huant, G. Auvert, F. Comin and J. Chevrier, *Nanoscale Res. Lett.* **5**, 1360 (2010).